

Retraction

Retracted: Mine Geological Environment Monitoring and Risk Assessment in Arid and Semiarid Areas

Complexity

Received 23 January 2024; Accepted 23 January 2024; Published 24 January 2024

Copyright © 2024 Complexity. This is an open access article distributed under the Creative Commons Attribution License, which permits unrestricted use, distribution, and reproduction in any medium, provided the original work is properly cited.

This article has been retracted by Hindawi following an investigation undertaken by the publisher [1]. This investigation has uncovered evidence of one or more of the following indicators of systematic manipulation of the publication process:

- (1) Discrepancies in scope
- (2) Discrepancies in the description of the research reported
- (3) Discrepancies between the availability of data and the research described
- (4) Inappropriate citations
- (5) Incoherent, meaningless and/or irrelevant content included in the article
- (6) Manipulated or compromised peer review

The presence of these indicators undermines our confidence in the integrity of the article's content and we cannot, therefore, vouch for its reliability. Please note that this notice is intended solely to alert readers that the content of this article is unreliable. We have not investigated whether authors were aware of or involved in the systematic manipulation of the publication process.

Wiley and Hindawi regrets that the usual quality checks did not identify these issues before publication and have since put additional measures in place to safeguard research integrity.

We wish to credit our own Research Integrity and Research Publishing teams and anonymous and named external researchers and research integrity experts for contributing to this investigation.

The corresponding author, as the representative of all authors, has been given the opportunity to register their agreement or disagreement to this retraction. We have kept a record of any response received.

References

- [1] J. Jin, C. Yan, Y. Tang, and Y. Yin, "Mine Geological Environment Monitoring and Risk Assessment in Arid and Semiarid Areas," *Complexity*, vol. 2021, Article ID 3896130, 10 pages, 2021.

Research Article

Mine Geological Environment Monitoring and Risk Assessment in Arid and Semiarid Areas

Jiaqi Jin, Chicheng Yan, Yixuan Tang, and Yilong Yin 

Miami College, Henan University, Kaifeng, Henan 475004, China

Correspondence should be addressed to Yilong Yin; sdq1202@henu.edu.cn

Received 23 April 2021; Revised 15 May 2021; Accepted 27 May 2021; Published 3 June 2021

Academic Editor: Zhihan Lv

Copyright © 2021 Jiaqi Jin et al. This is an open access article distributed under the Creative Commons Attribution License, which permits unrestricted use, distribution, and reproduction in any medium, provided the original work is properly cited.

Along with the accelerated shift of coal mining to the ecologically fragile west, the contradiction between coal resource development and ecological protection in the western arid and semiarid coal mining areas is rapidly intensifying. Based on the above background, this thesis takes the coal mining area in the arid and semiarid regions as an example; applies the theories of ecology, coal mining subsidence, geodesy, and ecological restoration; uses remote sensing in synthetic aperture radar (SAR), geographic information system (GIS), and mathematical modelling to reveal the ecological evolution law of the mining area; measures the ecological damage of the mining area; and then proposes a reasonable ecological restoration strategy. The surface deformation monitoring study in the study area shows that on the whole, some areas in the study area have different degrees of surface subsidence disasters, and the maximum surface subsidence value exceeds 800 mm. From the distribution of surface subsidence in the study area, surface subsidence disasters mainly occur in the eastern and central mountainous areas rich in coal resources, as well as in the mining areas west of the Yellow River, and the subsidence basins are distributed in a series of irregular concentric ovals. In terms of the scale of surface subsidence in the study area, a total of 230.03 km² of land in the study area showed surface subsidence hazards during the monitoring period, accounting for 13.78% of the total area of the study area, of which the area of severe subsidence was 44.98 km² (2.69%). The area of more serious subsidence area is 101.33 km² (6.07%), and the area affected by subsidence is 83.72 km² (5.01%).

1. Introduction

In 2015, coal consumption was 3.965 billion tons, accounting for 64% of the energy consumption structure, and the coal industry has made immeasurable contributions to the steady development of the national economy, but coal mining has caused damage to the ecological environment of mining areas while promoting economic development, thus directly threatening the ecological security and sustainable social development of mining areas [1]. The contradiction between mining resources development and ecological environment security is especially prominent in the western arid and semiarid areas [2]. The coal reserves in the western coal mining area account for more than 80% of China's coal reserves and are also the main coal-producing area in China, which has an important strategic position in the future energy development [3]. However, the dry climate, low

precipitation, strong evaporation, sparse vegetation, and lack of biodiversity in the western arid and semiarid regions make its fragile ecosystem inevitably accelerate land degradation and intensify soil erosion and desertification under the influence of mining activities, and mining disturbance may even make the ecosystem in the arid and semiarid regions break through the ecological recovery threshold and undergo irreversible changes [4].

In the process of resource extraction, the sharp increase in mining drainage and production water and mining ground fractures can lead to a significant drop in the groundwater level, thus causing ecological, environmental, and social problems such as the death of surface crops, the reduction of vegetation, and difficulties in water supply for humans and animals [5–10]. At the same time, the extraction process causes the movement, deformation, and discontinuous destruction of rock layers and ground, triggering

surface deformation accompanied by ground collapse, ground cracks, landslides, and other serious geological disasters [11]. The coal mining disturbances such as groundwater level drop, coal gangue accumulation, and surface subsidence will cause a series of ecological, environmental, and social problems such as landscape pattern change, intensification of human-land conflict, and loss of species diversity [12]. In recent years, the research on mining ecosystem environment using traditional passive optical remote sensing has been widely concerned by domestic and foreign scholars, such as the research on land-use/land-cover change based on remote sensing and the research on ecosystem evolution based on normalized difference vegetation index, landscape pattern index, and other ecological indicators [13]. Furthermore, the all-day, all-weather capability of active microwave remote sensing for monitoring minute deformation makes up for the limitations of optical remote sensing ecological monitoring [14]. The ecological monitoring technology based on active-passive remote sensing can realize a three-dimensional monitoring system with full spatial and temporal coverage for the ecological environment of the mining area, and the accurate and timely grasp of the ecological environment changes in the mining area is conducive to the formulation of scientific and reliable ecological restoration strategies, thus harmonizing the contradiction between mineral resources exploitation and ecological environmental protection and promoting the sustainable development of the mining area [15]. Based on this, this thesis takes the coal mining base in the arid and semiarid regions, for example, the Wuhai mining area, and uses the theories of ecology, coal mining subsidence, geodesy, ecological restoration, econometrics, and other methods, such as active radar remote sensing, passive optical remote sensing, GIS, and mathematical modelling, to analyze the arid and semiarid mining areas systematically [16]. It is of great significance to improve the ecological environment of coal mining areas and achieve sustainable development of regional ecology, economy, and society [17]. Using the mineral methods provides reliable guarantees for the production and livelihoods, while at the same time, the coal mines are accompanied by enormous environmental costs, and coal mines will occur continuously that brings serious imbalances to the ecology in some areas.

This thesis is based on the analysis and summary of academic research on arid and semiarid mining ecosystems, ecological environment remote sensing monitoring, quantitative ecological evaluation model, ecological restoration of mining areas, and so on [18–22]. It introduces optical remote sensing and radar remote sensing as monitoring means to study the mining ecosystem and evaluate the ecological environment monitoring results of mining areas [23–25]. It also uses GIS technology to zone the degree of damage to the ecological environment in the mining area and adopts targeted restoration and treatment strategies for different areas. The ecological factors response mechanism of mine ecosystem under mining disturbance is discussed; NDVI and ecological landscape pattern index are selected as the monitoring indicators of mine ecological disturbance according to the characteristics of mine ecosystem

disturbance; and the dynamic changes of vegetation cover and landscape ecology index in the study area in 2000, 2005, 2009, and 2015 are obtained according to remote sensing and econometric model to analyze and evaluate the ecosystem evolution process in the mining area. We have established an ecological monitoring system in arid and semi-arid mining areas to assess the degree of ecological damage in the mining area. By integrating land-use/land-cover changes, NDVI ecological monitoring index changes, and surface sedimentation in the mining area, the ecological damage evaluation model was established, and the study area was divided as lightly damaged, moderately damaged, and severely damaged areas according to different ecological damage levels, and its regional targeted restoration strategies and restoration technologies were proposed.

2. Mine Area Profile and Environmental Remote Sensing Data Processing

2.1. Overview of Arid and Semiarid Mining Areas. Table Mountain, Gander Mountain, and Wuhu Mountain are located in the eastern, central, and western parts of the study area, respectively. The overall topography of the region is high in the east and west and low in the middle. The landforms in the study area are divided into four categories: tectonic erosion of low and middle mountains, pre-mountain alluvial floodplain fan area, denuded hills, and alluvial terraces of the Yellow River, accounting for 40%, 30%, 20%, and 10% of the total area of the study area, respectively. The climate type of the study area is a temperate continental climate, with dry spring and little rain, hot summer and high temperature, and cold autumn and winter with little snow. The study area has abundant solar energy resources, with an annual average absorbed solar radiation energy of 155.8 kcal/cm^2 , an annual average sunshine duration of 3094.21 h, an annual average temperature of 9.96, extreme maximum and minimum temperatures reaching 40.20 and -36.60°C , respectively, and an extreme temperature difference of 76.80°C . The study area includes arid and semiarid zones, with low average annual precipitation and high evaporation; the average annual precipitation is 159.8 mm; the average annual evaporation is 3,289 mm; the average relative humidity is 41%; the average annual wind speed is 2.9 m/s; and the maximum wind speed can reach 33 m/s. The length of the Yellow River in the study area is about 105 km; the width is about 300–500 m; the depth is about 3–12 m; and the average annual runoff is 26.9 km^3 . According to the hydrological bureau of Inner Mongolia Autonomous Region, the groundwater reserves in the study area are 6.5 km^3 , and the available amount is 0.95 billion m^3 , and precipitation infiltration, Yellow River infiltration, recharge infiltration and condensate are the main sources of groundwater, as shown in Figure 1. The study area is very rich in mineral resources and has always been named “the sea of gold”. The study area is rich in 37 kinds of mineral resources, of which 25 kinds have been proven reserves, containing an economic value of more than 400 billion yuan. More than 80 mineral resources are exploited in the study area, and the mining products produced by them provide material security and power for the economic development of the study area.

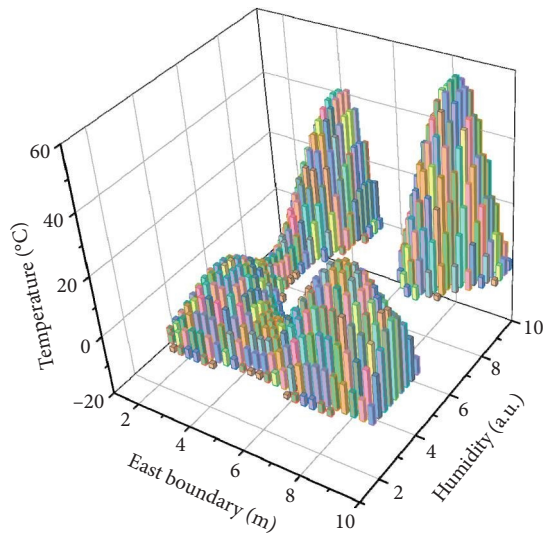


FIGURE 1: Distribution of humidity, temperature, and terrain in the study area.

The coal resource reserves in the study area are huge, with the current coal holding reserves of 4.43 billion tons. The coal resources in the study area are spatially and geographically concentrated, and due to the advantages of shallow burial of coal-bearing seams, the high heat content of coal, and thick coal seam aggregation, the Wuhai mining area is an important strategic energy site in China. The Wuhai mining area belongs to the Shandong hundred-million-ton coal production base, including the Haibowan mining area, the Wuda mining area, and the Hainan mining area, with more than 120 mine production sites.

The rich coal resources provide a reliable guarantee for the production and life of the people in Wuhai, while coal resources also contribute greatly to national and regional economic and social development but at the same time carry a huge environmental cost, with coal mining causing continuous and violent disturbance to the regional ecological environment, leading to serious imbalance in the ecological balance of some regions. According to the “Overall Plan for the Comprehensive Management of Coal Mining Area Disasters in Wuhai City” prepared by the Coal Authority in 2013, the mining area formed in Wuhai city is 26.9 km².

The geological environment survey of the city’s mines carried out in 2012 in Wuhai city shows that mining has formed 5.29 km² of ground subsidence area, 31.51 km² of open pit, 15.76 km² of solid waste accumulation, 28.48 km² of drainage field, and 28.48 km² the industrial waste disposal field. The industrial wasteland is 4.88 km². Divided by the formation period, the historical mine is 26.41 km², and the production mine due to geological environmental problems is 59.51 km². At the same time, air discharged into the tunnel from the mining area can easily cause spontaneous combustion of underground coal seams in nearby areas. The geological environment of mines, such as open pit and drainage field, not only occupies and destroys land resources, destroys the landscape of topography and

geomorphology, and triggers geological disasters such as collapse and mudflow but also leads to the destruction of aquifers, depletion of water resources, and decrease of groundwater level. The shantytowns built by the mine are affected by the ground subsidence and produce cracks, while the local production and life are seriously troubled by air pollution and garbage pollution, and the dirty, messy, and poor environment brings a lot of inconvenience to the residents’ life.

2.2. Data Sources and Preprocessing. The rapid development and wide application of 3S (RS, GIS, and GPS) technologies provide data support and technical support for research on land-cover change and ecological environment monitoring, among which remote sensing images are commonly used by scholars in regional land ecological monitoring research. This paper establishes a land-use classification system in the study area based on multisource remote sensing data through data collection and field survey and adopts the supervised classification method of support vector machine to obtain land-cover change data in different periods and evaluate the accuracy of land classification, and the classification results of remote sensing images can provide basic data for ecological environment changes in the study area. Since the differences in seasonal and temporal cumulative effects can lead to pseudo changes in land cover in the study area, remote sensing images with the same phase and time interval should be used as the data source for processing and analysis in the study area land-use change. In this thesis, by considering the cyclical characteristics of coal resource mining in the study area as well as land-use characteristics and data availability, the remote sensing images were selected on the basis of (1) preferring remote sensing images in June/July/August to facilitate the identification of forest and grassland, (2) selecting remote sensing images with cloudiness lower than 5%, and (3) selecting four remote sensing periods of August, September, and October 2010 and January 2015 in the study area data. The remote sensing data and other data selected for this thesis are shown in Table 1.

In this paper, professional software such as Arc GIS 10.2 geographic information platform and ENVI 5.3 remote sensing image processing platform provided by ESRI, the world’s largest GIS technology software developer, are selected for remote sensing data preprocessing. The preprocessing steps for Landsat TM/OLI images are radiometric correction, projection transformation, geometric correction, data fusion, and image cropping of the original images. The preprocessing process of remote sensing images is shown in Figure 2.

2.2.1. Multiband Combinations. In ENVI 5.3, the multi-spectral bands of remote sensing images of each period are combined into multiband image files. The images beyond the study area are cropped out according to the study area extent to improve the image preprocessing efficiency.

TABLE 1: Data type and acquisition.

Data type	Acquisition time	Data use	Data sources
Landsat TM	August 2010	Obtain land-cover change information	USGS
Landsat TM	September 2010		
Landsat TM	October 2010		
Landsat OLI	January 2015		

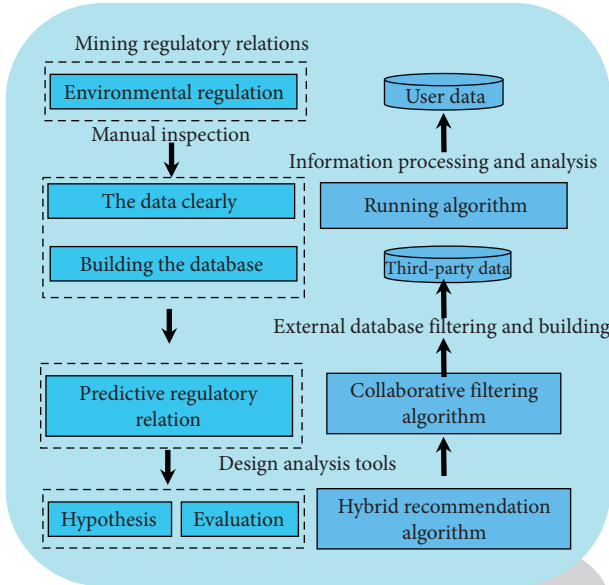


FIGURE 2: Image preprocessing flow chart.

2.2.2. Radiation Correction. Radiation correction is the process of removing the distortion of radiation brightness in remote sensing images due to sensor or detector characteristics, atmospheric effects, solar radiation, and so on. In this paper, the histogram equalization method is used for the radiometric correction of images. The histogram can automatically match the histogram of one display image data to another remote sensing image, which can effectively reduce the difference of brightness distribution of two remote sensing image pixels.

2.2.3. Projection Transformation. Based on the comprehensive consideration of the geographic location and area of the study area, the spatial data in this paper are uniformly converted to coordinates under the GIS software Arc GIS 10.2 environment, and all adopt the Xian80 coordinate system with the central longitude of 106°E and 3-degree division. The remote sensing imaging is influenced by the position and speed of remote sensing sensors as well as the rotation and curvature of the Earth, which leads to the difference between remote sensing images and the actual situation on the ground and geometric distortion. In remote sensing technology, geometric deformation of data is divided into nonsystematic and systematic. Systematic geometric deformation can be corrected using known sensor models, while nonsystematic geometric deformation is irregular, and geometric correction is needed to eliminate these nonsystematic geometric deformations.

2.2.4. Image Cropping. The purpose of image cropping is to remove areas outside of the study. According to the image cropping process of ENVI, it can be divided as regular cropping and irregular cropping. The former process is simpler and determines the cropping interval of the image based on the coordinates of two points in the upper left and lower right corners of the image. The latter involves in determining the boundary range of the cropped image using the already prepared irregular closure lines or manually drawn ROI polygons. In this paper, image cropping is carried out for the four remote sensing images of 2000, 2005, 2009, and 2015 using the administrative boundary of Wuhai District according to the orientation of the study area. First, polygons are generated in Arc GIS10.2 according to the administrative boundary of the study area, converted into raster image files, and the irregular cropping of images is achieved by setting new value to 1 in the region of interest and new value to 0 outside the region through masking operation.

2.3. Geological Testing and Environmental Assessment. Remote sensing classification is an important step in the generation of land-use classification maps from remote sensing images. The classification system of land use in the study area must be determined before the classification. Land-use type is the result of human production and lifestyle transforming the land-use landscape, and there are differences in land-use types in different geographical locations, climatic characteristics, and leading industrial regions. Therefore, the basic standard of land use classification system should be used as a reference basis, combined with the characteristics of land use types in arid and semi-arid mining areas to determine the land use classification system in the study area. In this paper, based on the field survey of land use in the study area, with reference to the “Regulations for Dynamic Remote Sensing Monitoring of Land Use” and “Classification of Current Land Use”, and based on the identifiable resolution of Landsat remote sensing satellite images, the land-use types in the study area are classified into five categories: arable land, forest and grassland, water area, construction land, and coal mining land (Table 2).

2.3.1. Image Spectral Feature Analysis. The spectral response characteristics of remote sensing images are usually reflected by the reflectance values of features on multispectral images, and the spectral characteristics of features are the physical basis for the interpretation and classification of remote sensing images. In general, the reflectance of the same feature at each stage is different, and the reflectance of different features on the same waveband image is also

TABLE 2: Land-use classification system and assignment of remote sensing images in the study area.

Name of land type	Significance	Score
Arable land	Dryland, watered land, and paddy field	20
Forest lawn	Grassland and woodland	30
Waters	Rivers, pond water, and lakes	10
Construction land	Transportation land and urban land	20
Coal mining land	Coal mine open pit	10

different from each other. Image classification must be based on a comprehensive understanding of the spectral characteristics of various types of features at different wavelengths. Before image classification, typical samples of each type of feature were selected on the pre-processed TM images of 2015 in the study area, and their spectral profiles were analyzed to find out the spectral characteristics of the features. After the comparative analysis of the visual effects of different schemes of pseudo color synthesis, it was found that Bands 5, 4, and 3 synthesized better, with colorful and informative images. Bands 5, 4, and 3 were given red, green, and blue colors, respectively, and the obtained image colors were close to the real colors, which were easy to interpret visually and easy to interpret the images.

2.3.2. Image Texture Feature Analysis. As an important method for feature recognition, texture feature extraction analysis can reflect the relationship between landscape and features, while the integration of texture information features is beneficial to improve the accuracy of land-use classification. The commonly used texture measures in image texture features are entropy, contrast, second moment, correlation, energy, variance, mean, and so on. In this study, four texture measures, entropy, contrast, second moment, and correlation, were selected for texture feature extraction of images, as shown in Table 3.

The supervised classification method is one of the main methods for spectral-based remote sensing image classification. The basic principle of supervised classification, also called the training classification method, is to use the identified classification sample image elements to judge the image land-use types, and its identification and classification methods include maximum likelihood method, minimum distance method, Marxian distance method, neural network method, parallel hexahedron method, support vector machine method, and so on. The supervised classification method first determines the reliable land-use types in some areas of remote sensing images through effective visual interpretation of high-resolution images and actual field investigation and establishes the classification system. When the training samples are qualified, the training samples can be trained to discriminate functions based on scientific and suitable classification methods, and finally, the discriminating functions qualified by training can be used to discriminate the utilization types of other pixels, so as to complete the classification of remote sensing images. The supervised classification of remote sensing images includes the following six steps, as shown in Figure 3.

TABLE 3: Commonly used texture measures.

No	Parameter indicators	Specific gravity	Select assignment
1	Entropy	20	1
2	Contrast	20	1
3	Second moment	20	1
4	Correlation	20	1
5	Energy	10	—
6	Variance	5	—
7	Mean	5	—

In this paper, a supervised classification using the support vector machine method was used to study the land-use classification of the study area for the years 2000, 2005, 2009, and 2015. Support vector machine (SVM) is an automatic computer learning algorithm based on the principle of statistical analysis. Support vector machines can actively discover support vectors that have greater discriminatory power in classification and build classifier models based on these support vectors. Support vector machine method can maximize the difference between each category, so the method has high accuracy and good research value.

2.4. Hazard Assessment and Radar Detection. The degree of accuracy of remote sensing image classification directly affects the reliability of the classification results, so the evaluation of remote sensing classification accuracy is an important part of land-use information extraction and classification. In general, the basic principle of classification accuracy evaluation is to compare and analyze the classification results with field research data or other reliable data, so as to evaluate the accuracy and precision of the classification results. The methods include confusion matrix, overall classification accuracy, Kappa coefficient, misclassification error, omission error, mapping accuracy, and user accuracy. The Kappa coefficient, producer accuracy, and user accuracy are utilized in this thesis for the accuracy evaluation of classification results. The classification accuracy of the supervised classification method based on the support vector machine method is high, and its Kappa coefficient is above 0.8. Therefore, the land-use classification results of the four-time phases are consistent with the actual ground reference types and meet the needs of this paper.

Synthetic aperture radar interferometry (interferometric synthetic aperture radar) uses an electromagnetic wave sensor to transmit microwave signals to the ground target area and then accepts the echo signal emitted by the target to obtain two radar images of the target area, and among the target point and the location of the two acquired radar images in space, there is a mathematical geometric relationship, so the phase difference will be generated in the stripe map after the interference processing of the two images, and then through this interference phase difference, combined with the sensor height from the ground, microwave wavelength, microwave incidence angle, and other data can accurately invert and measure the three-dimensional location and change information of each feature point in the ground target area. Sensor-carrying vehicles are divided into

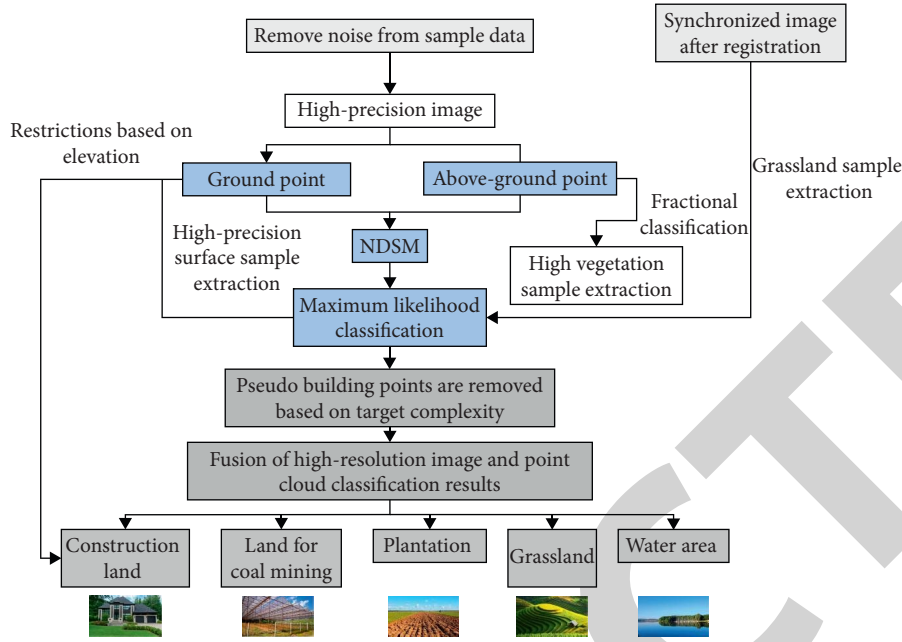


FIGURE 3: Supervised classification operation flow.

two types: aircraft and satellite; airborne SAR data are generally observed simultaneously by two sets of microwave signal receivers (single track), and satellite-borne SAR data are observed by two transmissions of microwave signals from shorter baselines (repeated track). In this paper, the geometric principle of synthetic aperture radar is introduced as an example of the repetitive orbit interferometry mode of satellite-borne radar.

Let P be the observation target feature, O_1 and O_2 be the positions of the SAR sensors when the satellite repeatedly observes the target area along different orbits twice, h be the horizontal elevation of point P , H and θ be the platform height and incidence angle of the SAR satellite at the time of the first observation, respectively, and Q be the spatial baseline of the sensors for both observations. α is the inclination angle of the baseline Q along the horizontal direction, and the decomposition of the spatial baseline in the direction perpendicular to the component of the decomposition of the spatial baseline in the line of sight direction is called the vertical baseline, and the component of the decomposition in the parallel to the line of sight direction is called the parallel baseline, whose mathematical expressions are as follows:

$$\begin{aligned} Q_{\perp} &= Q \frac{\cos(\alpha - \theta) + 1}{\cos(\alpha - \theta) - 1}, \\ Q_{\parallel} &= Q \frac{\sin(\alpha - \theta) + 1}{\sin(\alpha - \theta) - 1}. \end{aligned} \quad (1)$$

When the SAR satellite conducts Earth observation, it first actively sends microwave radar signals to the ground target and then receives the microwave signals after reflecting through the ground surface, and the echo signals contain both intensity and also phase information. The SAR intensity map of the target area can be obtained by the

different intensity of the reflected microwaves from the ground, while the phase information can be used to invert the elevation information of the target area when the wavelength and period of the microwaves are determined, which is the key of in SAR technology. Generally, before the interferometric processing, the two observed images are defined as the master image (Master) and the secondary image (Slave), and then the echo signals (containing intensity and phase information) of point P in the master and secondary images are defined as follows:

$$\begin{aligned} u(r_1) &= ar_1 \exp(i\phi r_1), \\ u(r_2) &= ar_2 \exp(i\phi r_2), \end{aligned} \quad (2)$$

where ar_1 and ar_2 denote the magnitude of the two observed echo amplitudes, and ir_1 and ir_2 denote the two observed echo phase information. According to the backscattering characteristics of the features, the SAR signal echo phase can be divided into geometrically regular reflection phase and random phase and thus can be converted as follows:

$$\begin{aligned} \phi r_1 &= \frac{4\pi r_1}{1 + \lambda} + \frac{1 + \phi_1}{1 - \phi_1}, \\ \phi r_2 &= \frac{4\pi r_2}{1 + \lambda} + \frac{1 + \phi_2}{1 - \phi_2} 4\pi. \end{aligned} \quad (3)$$

The random phase is random for a single image, but after the primary and secondary image interference processing, the random phase and the path difference Δr have a certain relationship as follows:

$$\phi = - \left(\frac{4\pi \cdot (r_1 - r_2)}{1 + \lambda} \right). \quad (4)$$

After the interference processing, the phase information obtained is not the true phase due to the phase entanglement

phenomenon caused by the period, so phase unwinding must be performed to remove the effect of the period H as follows:

$$h - H = -r_1 \frac{(1 - \sin \theta)}{1 + \cos \theta},$$

$$\cos(\lambda - \theta) = \frac{r_2^2 - r_1^2}{r_2^2 + r_1^2} \cdot 2r, \quad (5)$$

$$r_2 - r_1 = \Delta r.$$

The joint solution of the four equations leads to the derivation of the elevation h of the ground target P as a function of the interference phase as follows:

$$H - h = \frac{(Q - (\lambda/4\pi(1 - \lambda)))(Q + (\lambda/4\pi(1 - \lambda)))}{(\lambda/4\pi(1 - \lambda)) + \cos(\lambda - \theta)}. \quad (6)$$

3. Results and Analysis

This study relies on the results of the second land survey change library in the study area and the four-phase remote sensing images based on supervised postclassification to conduct land-use change analysis. Using the postclassification statistics function of ENVI5.3, the composition structure of land-use types in the mining area was obtained statistically, as shown in Figure 4.

The change in land-use structure in the mining area is mainly manifested in the following areas:

- (1) The study area includes the semiarid grassland area, which is related to the geographical location, and the main land-use type of the study area is grassland, and the area of forest grassland accounts for more than 50% of the total area of the study area. From 2000 to 2009, the area of forest grassland showed a decreasing trend, and the proportion decreased from 66.44% to 44.91%, but the area increased from 2009 to 2015, but the overall trend was decreasing. From the land-use distribution map, grasslands were mainly distributed in the south, central, and northeastern parts of the study area and were concentrated in a continuous distribution.
- (2) Construction land and coal mining land are the second-largest land-use types in the study area. Construction land showed an increasing trend during 2000–2015, increasing from 146.76 km² in 2000 to 266.77 km² in 2015 and becoming the second-largest land type from the third-largest land type in the study area. Coal mining land area also showed an increasing trend during 2000–2015, from 55.13 km² to 161.93 km², and its share increased from 3.14% to 9.23%.
- (3) The third-largest land type in the study area is cropland. The area of cultivated land in the study area showed a decreasing trend during 2000–2005 and maintained an increasing trend during 2005–2015, with an overall increase from 8% to 15%.

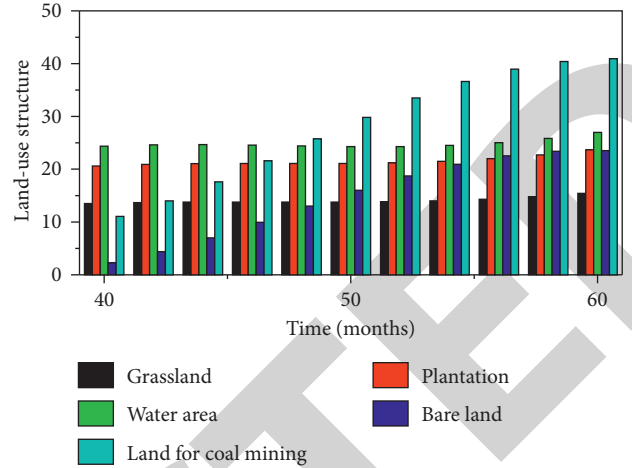


FIGURE 4: Land-use structure of the study area.

Cultivated land in the study area was distributed along the east and west sides of the Yellow River channel mainly concentrated in the western part of the study area. Bare land showed an increasing trend during 2000–2005, with the proportion increasing from 11.69% to 24.14% and then decreased sharply from 2009–2015 from 20.47% to 6.14% in 2009.

- (4) The water area in the study area remained basically unchanged during 2000–2009, accounting for about 2% of the total study area and increased to 68.72 km² during 2009–2015, with the proportion increasing to 3.92%.

The analysis of the magnitude of land-use change in the study area is used to reflect the evolution of the area of each land-use type in the study area during the study period, including the total magnitude of change of each land-use type and the average annual magnitude of change of the area of each land-use type, as shown in Figure 5.

The largest change in forest grassland was followed by construction land, cropland, and coal mining land. The area of forest and grassland decreased by 279.93 km² during the whole study period, 221.80 km² during 2000–2005, 155.87 km² during 2005–2009, and 97.74 km² during 2009–2015. From 2000 to 2009, natural grassland and woodland were created due to the mining of raw coal, especially the mining of open-pit coal mines. During the “12th five-year plan” period, Wuhai city actively promoted ecological environment construction, took the opportunity to create a national model greening city and national garden city, and vigorously implemented key ecological projects such as natural forest resources protection and Beijing-Tianjin wind and sand source control, which increased the area of forest and grassland.

Based on the results of the classification of land-use types in the study area in 2000, 2005, 2009, and 2015 (as shown in Figure 6), the land-use changes in the study area from 2000 to 2015 were obtained by combining the calculation models of integrated land-use dynamics and single land-use dynamics.

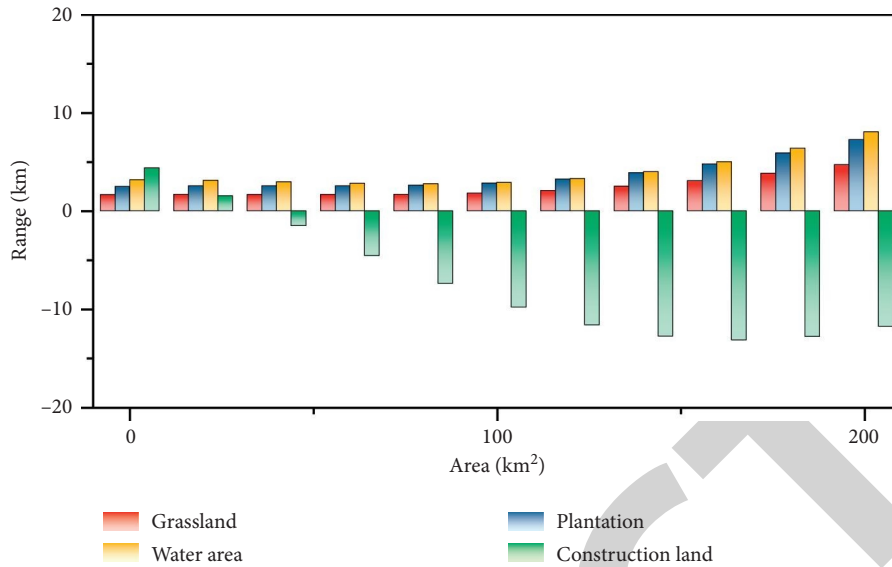


FIGURE 5: Land-use type area change.

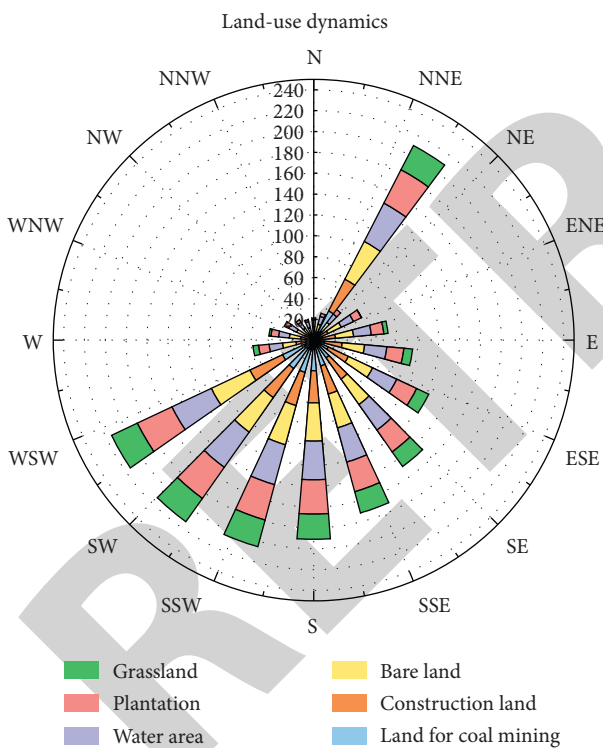


FIGURE 6: Land-use dynamics in the study area.

Single land-use dynamic attitude: From 2000 to 2005, the annual growth rate of bare land is the largest, 21.29%, followed by construction land, with an annual growth rate of 10.2%; the annual decrease rate of arable land is the largest, -10.3%, followed by grassland, with an annual change rate of -3.81%. On the one hand, the strong demand for construction land brought by social and economic development, and on the other hand, along with the mining of coal

resources, the ecological environment continues to deteriorate, resulting in the continuous decrease of ecological land such as arable land and grassland and the continuous increase of bare land. The rate of change of arable land from 2005 to 2009 is the most obvious, contrary to the decrease between 2000 and 2005, with an annual growth rate of 45.16%, which is due to the treatment projects of saline and sandy land in the study area, and the conversion of bare land into agricultural production land such as grape plantation base; the change of coal mining land is also obvious, with the second single-motion attitude of 19.98%. This indicates that the scale of coal resources mining has been expanding from 2005 to 2009; watershed and forested land decreased significantly from 2005 to 2009, with a single-motion attitude of -8.60% and -4.13%, respectively.

Comprehensive land-use dynamics: From the calculation results, it can be seen that the comprehensive land-use dynamics from 2000 to 2005 and 2005 to 2009 were similar, 3.24% and 3.29%, respectively, with frequent changes in land-use types, and the comprehensive land-use dynamics from 2009 to 2015 was 2.63%, which was not much different from the previous two phases. From the whole study period, the comprehensive land-use dynamic attitude was 3% in the overall scope of the study area from 2000 to 2015, and the land-use change was unstable.

It can be seen that the land degradation in the mining area of Wuhai due to mining activities mainly caused a total decrease of 0.011 in NDVI from 2000 to 2009, with a decrease ratio of 22.9%, including 0.008 and 0.003 from 2000 to 2005 and 2005 to 2009, respectively; With the layout of the comprehensive mine ecological environment management project in the study area, the NDVI value from 2009 to 2015 retraced upward by 0.004, accounting for 10.8% of the NDVI in 2009. The changes of NDVI mean and standard deviation in the study area are shown in Figure 7.

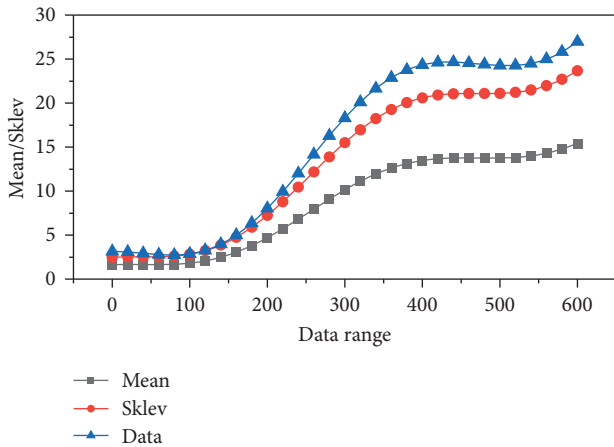


FIGURE 7: NDVI variation curve in the study area.

4. Conclusion

Based on the mechanism of ecosystem disturbance in arid and semiarid mining areas, this study analyzed the land-use/land-cover change, vegetation-cover change, and landscape pattern change in the study area from 2000 to 2015 and conducted a surface deformation monitoring test to analyze the cumulative surface deformation results of the study area from January to November 2015. Based on this, the ecological damage evaluation model was constructed by integrating the surface vegetation-cover status and surface deformation monitoring results, and the ecological damage degree in the study area was zoned, and different ecological restoration strategies were proposed for different damage degree areas in the study area. The study of land-use/land-cover change showed that the land-use conversion in the study area was more frequent throughout the study period; the vegetation-cover level was continuously reduced; the landscape fragmentation was continuously enhanced; and the regional ecosystem was in a bad development situation. The SAR intensity map of the target area can be obtained by the different intensity of the reflected microwaves from the ground, while the phase information can be used to invert the elevation information of the target area when the wavelength and period of the microwaves are determined, which is the key of in SAR technology. The vegetation cover in the study area showed obvious changes in time series and spatial distribution, from 2000 to 2009, the range of medium and high vegetation-cover areas gradually shrank; the area of areas with low vegetation cover gradually increased; and the degree of landscape diversity increased.

Data Availability

The data used to support the findings of this study are available from the corresponding author upon request.

Conflicts of Interest

The authors declare that they have no known conflicts of interest or personal relationships that could have appeared to influence the work reported in this paper.

References

- [1] J. Wang, Y. Yin, H. Yu, C. Jiang, and Y. Wan, "Remote sensing monitoring of mine geological environment in zhejiang province based on RS and GIS," *Remote Sensing for Land & Resources*, vol. 32, no. 1, pp. 232–236, 2020.
- [2] Z. Yang, W. Li, Y. Pei, W. Qiao, and Y. Wu, "Classification of the type of eco-geological environment of a coal mine District: a case study of an ecologically fragile region in western China," *Journal of Cleaner Production*, vol. 174, pp. 1513–1526, 2018.
- [3] J. Wang, "Typical model analysis of mine geological environment restoration and management in zhejiang province based on domestic high-resolution satellite data," *Remote Sensing for Land & Resources*, vol. 32, no. 3, pp. 216–221, 2020.
- [4] B. A. Cymes and M. P. S. Krekeler, "Using HR-TEM for geological environment investigation: a case study of silver nanoparticles associated with mine waste in a world heritage site," *Microscopy and Microanalysis*, vol. 24, no. S1, pp. 1708–1709, 2018.
- [5] R. Ahmadi, M. El May, and M. Dlala, "Ultimate slope design in open pit phosphate mine using geological and geo-mechanical analysis: case study of jebel jebbeus," *Arabian Journal of Geosciences*, vol. 12, no. 9, pp. 1–14, 2019.
- [6] M. Marcisz, K. Probiez, and M. Ostrowska-Lach, "3D representation of geological observations in underground mine workings of the upper Silesian coal basin," *Journal of Sustainable Mining*, vol. 17, no. 1, pp. 34–39, 2018.
- [7] J. Yamaguchi, M. Naoi, M. Nakatani et al., "Emergence and disappearance of very small repeating earthquakes on a geological fault in a gold mine in South Africa," *Tectonophysics*, vol. 747–748, pp. 318–326, 2018.
- [8] V. Nesterovskiy, V. Ishkov, and Y. Kozii, "Toxic and potentially toxic elements in the coal of the seam c8h of the "blagodatna" mine of pavlohrad-petropavlivka geological and industrial area," *Visnyk of Taras Shevchenko National University of Kyiv. Geology*, vol. 1, no. 88, pp. 17–24, 2020.
- [9] Y. Guo, N. Liu, X. Huang, and J. Li, "Removal algorithm of horizontal noise for echoes in mine geological radar," *Arabian Journal of Geosciences*, vol. 13, no. 15, pp. 1–10, 2020.
- [10] Z. Tao, F. Fan, X. Yang, Z. Guo, G. Li, and X. Meng, "Prediction of deep rock mass quality and spatial distribution law of open-pit gold mine based on 3D geological modeling," *Geotechnical and Geological Engineering*, vol. 39, pp. 3221–3238, 2021.
- [11] G. Yang, "Name index," *Democratic Federalism*, vol. 10, no. 5, pp. 417–424, 2020.
- [12] T. R. Câmara, R. Scheffer Leal, and R. De Lemos Peroni, "Accounting for operational dilution by incorporating geological uncertainties in short-term mine planning," *Dyna*, vol. 87, no. 213, pp. 178–183, 2020.
- [13] M. Quigley and R. Dimitrakopoulos, "Incorporating geological and equipment performance uncertainty while optimising short-term mine production schedules," *International Journal of Mining, Reclamation and Environment*, vol. 34, no. 5, pp. 362–383, 2020.
- [14] P. Rajmeny and R. Shriali, "Use of radar technology to establish threshold values of blast vibrations triggering sliding of geological faults at a lead-zinc open pit mine," *International Journal of Rock Mechanics and Mining Sciences*, vol. 113, pp. 142–149, 2019.
- [15] H. Villena, "EL toro gold mine (Peru): geological features and perspectives," *Visnyk of Taras Shevchenko National University of Kyiv. Geology*, vol. 2, no. 81, pp. 63–69, 2018.

- [16] F. De Santis, I. Contrucci, J. Kinscher, P. Bernard, V. Renaud, and Y. Gunzburger, "Impact of geological heterogeneities on induced-seismicity in a deep sublevel stoping mine," *Pure and Applied Geophysics*, vol. 176, no. 2, pp. 697–717, 2019.
- [17] C. Birch, "Geological mapping and modelling training in the University of the Witwatersrand Mine Tunnel, South Africa," *Journal of The South African Institute of Mining and Metallurgy*, vol. 118, no. 8, pp. 809–814, 2018.
- [18] A. Флоров and A. Florov, "Prediction of hazardous geological process development in open mine working using information technologies," *Bulletin of Bryansk State Technical University*, vol. 2018, no. 10, pp. 72–77, 2018.
- [19] C. Zhang, C. Pu, R. Cao, T. Jiang, and G. Huang, "The stability and roof-support optimization of roadways passing through unfavorable geological bodies using advanced detection and monitoring methods, among others, in the sanmenxia bauxite mine in China's Henan province," *Bulletin of Engineering Geology and the Environment*, vol. 78, no. 7, pp. 5087–5099, 2019.
- [20] Z. Wang, Z. Huang, J. T. Brosnahan et al., "Ru/CeO₂ catalyst with optimized CeO₂ support morphology and surface facets for propane combustion," *Environmental Science & Technology*, vol. 53, no. 9, pp. 5349–5358, 2019.
- [21] G. Dong, W. Wei, X. Xia, M. Woźniak, and R. Damaševičius, "Safety risk assessment of a Pb-Zn mine based on fuzzy-grey correlation analysis," *Electronics*, vol. 9, no. 1, p. 130, 2020.
- [22] W. Yang, Y. Zhao, D. Wang, H. Wu, A. Lin, and L. He, "Using principal components analysis and IDW interpolation to determine spatial and temporal changes of surface water quality of Xin'anjiang River in Huangshan, China," *International Journal of Environmental Research and Public Health*, vol. 17, no. 8, p. 2942, 2020.
- [23] Y. Chen, W. Zheng, W. Li, and Y. Huang, "Large group activity security risk assessment and risk early warning based on random forest algorithm," *Pattern Recognition Letters*, vol. 144, pp. 1–5, 2021.
- [24] W. Wei, Q. Ke, J. Nowak, M. Korytkowski, R. Scherer, and M. Woźniak, "Accurate and fast URL phishing detector: a convolutional neural network approach," *Computer Networks*, vol. 178, no. 10, Article ID 107275, 2020.
- [25] Y. Li and J. Yang, "Few-shot cotton pest recognition and terminal realization," *Computers and Electronics in Agriculture*, vol. 169, no. 6, Article ID 105240, 2020.